

PCCP

Physical Chemistry Chemical Physics

Accepted Manuscript

This article can be cited before page numbers have been issued, to do this please use: L. CHAN, G. R. Hutchison and G. M. Morris, *Phys. Chem. Chem. Phys.*, 2020, DOI: 10.1039/C9CP06688H.



This is an Accepted Manuscript, which has been through the Royal Society of Chemistry peer review process and has been accepted for publication.

Accepted Manuscripts are published online shortly after acceptance, before technical editing, formatting and proof reading. Using this free service, authors can make their results available to the community, in citable form, before we publish the edited article. We will replace this Accepted Manuscript with the edited and formatted Advance Article as soon as it is available.

You can find more information about Accepted Manuscripts in the [Information for Authors](#).

Please note that technical editing may introduce minor changes to the text and/or graphics, which may alter content. The journal's standard [Terms & Conditions](#) and the [Ethical guidelines](#) still apply. In no event shall the Royal Society of Chemistry be held responsible for any errors or omissions in this Accepted Manuscript or any consequences arising from the use of any information it contains.

Cite this: DOI: 00.0000/xxxxxxxxxx

BOKEI: Bayesian Optimization Using Knowledge of Correlated Torsions and Expected Improvement for Conformer Generation

Lucian Chan,^a Geoffrey R. Hutchison,^b and Garrett M. Morris^{*a}Received Date
Accepted Date

DOI: 00.0000/xxxxxxxxxx

A key challenge in conformer sampling is finding low-energy conformations with a small number of energy evaluations. We recently demonstrated the Bayesian Optimization Algorithm (BOA) is an effective method for finding the lowest energy conformation of a small molecule. Our approach balances between *exploitation* and *exploration*, and is more efficient than exhaustive or random search methods. Here, we extend strategies used on proteins and oligopeptides (e.g. Ramachandran plots of secondary structure) and study the correlated torsions in small molecules. We use bivariate von Mises distributions to capture correlations, and use them to constrain the search space. We validate the performance of our new method, Bayesian Optimization with Knowledge-based Expected Improvement (BOKEI), on a dataset consisting of 533 diverse small molecules, using (i) a force field (MMFF94); and (ii) a semi-empirical method (GFN2), as the objective function. We compare the search performance of BOKEI, BOA with Expected Improvement (BOA-EI), and a genetic algorithm (GA), using a fixed number of energy evaluations. In more than 60% of the cases examined, BOKEI finds lower energy conformations than global optimization with BOA-EI or GA. More importantly, we find correlated torsions in up to 15% of small molecules in larger data sets, up to 8 times more often than previously reported. The BOKEI patterns not only describe steric clashes, but also reflect favorable intramolecular interactions such as hydrogen bonds and π - π stacking. Increasing our understanding of the conformational preferences of molecules will help improve our ability to find low energy conformers efficiently, which will have impact in a wide range of computational modeling applications.

1 Introduction

Many molecules can adopt multiple geometrically-distinct conformers. Considerable effort has been devoted to understanding the influence of structure on function, notably in the fields of protein folding, and protein-ligand binding^{1–3}. Finding the energetically-lowest conformation of a small molecule is a common task in computational chemistry^{4,5}. Here, we introduce a new search method that extends our previously proposed search strategy, Bayesian Optimization Algorithm, BOA⁶, by incorporating prior knowledge of correlated adjacent pairs of torsional angles.

We recently showed BOA tends to find the lowest energy conformation of small to medium organic molecules more efficiently than both an exhaustive systematic search, Confab⁷, and a uni-

form random search, when evaluated using a “fixed-rotor approximation” and the MMFF94 force field⁶. BOA required an order of magnitude fewer energy evaluations than these methods to find the lowest energy conformation. Drawing from statistical mechanics, BOA begins with an initial estimate of the probability of likely dihedral angles (e.g. 60°, 120°, 180°, etc.) and updates these probabilities by evaluating a new point on the potential energy surface (PES). In this way, BOA “learns” the most likely dihedral angles of a molecule from all previous observations, and determines the next query point based on the model’s uncertainty. This approach balances *exploration* and *exploitation*, and prevents the search from being trapped in local minima. However, BOA suffers from two limitations: one is that it tends to unnecessarily sample high energy regions of the potential energy surface. A second is that the Gaussian Process (GP) regression is used as a surrogate model, which is well-known to have high computational complexity, although recent studies⁸ have shown the asymptotic complexity of the exact GP inference can be reduced to $O(N^2)$, where N is the total number of energy evaluations. Here, we introduce a new *knowledge-based* acquisition function to address the first issue. Although GP has high computational complexity, we still use it as the surrogate model in this work. Its

^a Address, Department of Statistics, University of Oxford, 24-29 St Giles, Oxford, OX1 3LB, UK.; E-mail: garrett.morris@stats.ox.ac.uk

^b Address, Department of Chemistry and Chemical Engineering, University of Pittsburgh, 219 Parkman Avenue, Pittsburgh, PA 15260, USA.; E-mail: geoffh@pitt.edu

† Electronic Supplementary Information (ESI) available: All the data and code will be available online and GitHub <https://github.com/lucianlschan/Conformer-Geometry-v2>. See DOI: 10.26434/chemrxiv.9209213.

well-calibrated model of uncertainty is heavily used to guide the sampling on the PES in this work.

Various knowledge-based methods^{9–12} have been proposed for (diverse) conformer generation. These methods utilize the torsional preferences in guiding conformer sampling and the torsion rules are typically derived from databases of experimental X-ray crystal structures, such as the Protein Data Bank (PDB)¹³ and the Cambridge Structural Database (CSD)¹⁴, although they can also be derived from computed structures. Context and nearest neighbour effects are generally ignored in the torsion rules: each dihedral is treated as an independent free rotor¹.

Structural information about adjacent and proximal rotatable bonds can, however, be crucial for conformer generation, as these torsion angles are naturally constrained. This can help to reduce steric clashes, retain π -conjugation, align intramolecular hydrogen bonds, or preserve other similar non-covalent interactions. For instance, Fig. 1b shows the computed MMFF94 potential energy surface for 5-phenylthioquinazoline-2,4-diamine, with light blue indicating conformations with low energies. Due to steric clashes, the neighboring dihedral angles are clearly correlated and thus the conformational search can be greatly focused on the most favorable regions of the state space by incorporating this information. Even in a simpler molecule such as *ortho*-1,1':2',1''-terphenyl, there are correlations between non-neighboring dihedral angles due to steric clashes (Fig. 1d).

In this work, we examine the distributions of correlated torsions in (i) X-ray crystal structures; (ii) the lowest-energy conformations from MMFF94; and (iii) the lowest energy conformations from an approximate quantum method, GFN2. We analyze the distributions of the correlated torsions in the lowest-energy conformations computed first by MMFF94, and then by GFN2, and use these distributions to constrain the search space in Bayesian optimization using a modified acquisition function. We show that this significantly improves the efficiency of the search for low-energy conformations. We also show that correlated dihedral angles are common in organic small molecules.

2 Material and Methods

2.1 Knowledge-based Method

Guba *et al.*¹⁵ derived a set of rotatable bond SMARTS patterns that are used in RDKit's¹⁶ Experimental-Torsion Distance Geometry with basic Knowledge (ETKDG) algorithm¹⁷, and also in BOA⁶, the predecessor of our new method, BOKEI. This library only considered substructures consisting of a single rotatable bond. We expanded this set of patterns to consider correlated torsions in substructures consisting of two adjacent rotatable bonds.

2.1.1 Correlated Torsion Rules

We enumerated all possible pairs of rotatable bond SMARTS patterns as defined in the library of Guba *et al.*¹⁵, and counted the frequencies of the corresponding pairs of torsion angles observed in ligands having five or fewer rotatable bonds in the Crystallography Open Database (COD)^{18,19}. We excluded pair patterns

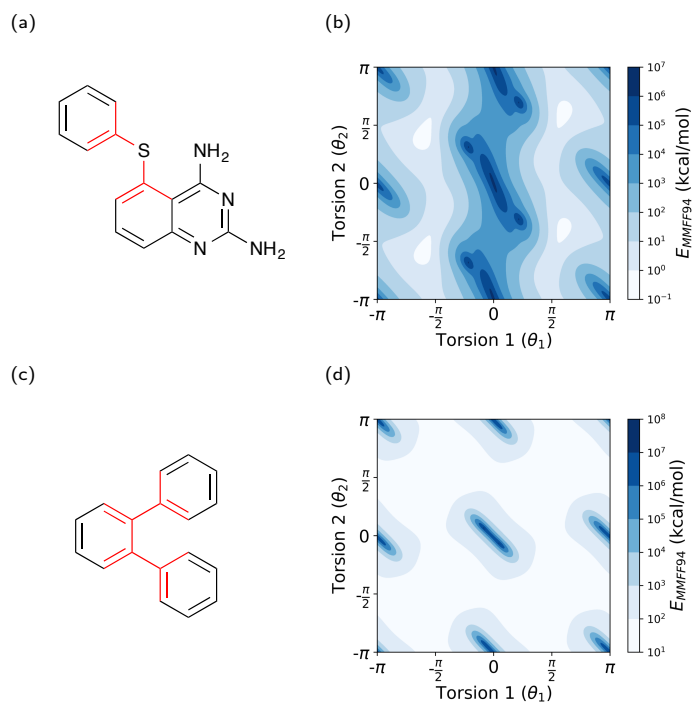


Fig. 1 (a) 5-Phenylthioquinazoline-2,4-diamine. (b) MMFF94 potential energy landscape for 5-Phenylthioquinazoline-2,4-diamine. (c) *ortho*-1,1':2',1''-terphenyl. (d) MMFF94 potential energy landscape for *ortho*-1,1':2',1''-terphenyl. The areas in light blue show the lowest-energy regions. Torsion angles are measured in radians. The correlated torsions in the molecules are highlighted in red.

with fewer than 100 observations, resulting in 19 correlated torsion patterns, including one SMARTS pattern suggested by Cole *et al.*⁹ (see Appendix 1 Table S1). The remaining substructures defined by Cole *et al.* were discarded due to insufficient observations in our dataset. Future work will expand on this initial set as discussed below.

For molecules that contain any matches of the derived SMARTS patterns, we calculated the lowest energy conformation and recorded the corresponding torsion angles. We performed the calculations with two energy functions: (i) a force field, MMFF94²⁰, and (ii) a semi-empirical method, GFN2^{21,22}. We then modeled the observed torsion distribution with bivariate von Mises mixture models for all three sources of structure (X-ray crystal structure, MMFF94, and GFN2) separately. Details of the calculations and models can be found in Appendix 2. The bivariate von Mises distribution has been used to model torsion angles in protein structures^{23–25}. There are two advantages of using this distribution for correlated torsions: (i) it can model correlated torsions that cannot be described by a simple clash term; and (ii) it can be easily integrated with existing conformer sampling schemes, such as distance geometry²⁶.

2.2 Bivariate von Mises Distribution and Mixture Models

The bivariate von Mises distribution is a probability distribution that can be used to jointly model two angular variables (θ_1 and θ_2). It can be thought of as an analogue of the bivariate normal

distribution on a torus. In particular, we used the cosine variant of the von Mises distribution, which is as follows:

$$f(\theta_1, \theta_2) \propto \exp(\kappa_1 \cos(\theta_1 - \mu) + \kappa_2 \cos(\theta_2 - \nu) - \kappa_3 \cos(\theta_1 - \mu - \theta_2 + \nu)) \quad (1)$$

where the parameters (μ , ν) and (κ_1 , κ_2) in the model represent the mean, and concentrations respectively. (κ_3) is a parameter controlling the correlation.

The bivariate von Mises distribution can be unimodal or bimodal under different conditions (see Appendix 2). A single bivariate von Mises distribution is not sufficient to capture the multimodality of the torsional preferences. We used mixture models (Eq. 2) to describe the torsional preference entirely; the probability, $P(\theta_1, \theta_2)$ of observing the pair of torsion angles, θ_1 and θ_2 , is given by:

$$P(\theta_1, \theta_2) = \sum_{i=1}^K w_i f_i(\theta_1, \theta_2) \quad (2)$$

where K is the number of components in the model, and w_i is the weight of each component. The estimation procedure of the parameters of the mixture models are explained in Appendix 2.

We should note that the bivariate von Mises mixture model requires sufficient data to accurately describe torsional preferences, so cases with small numbers of observations were excluded in this work. This limits the current performance of our algorithm, and we discuss some potential solutions in Section 3.7.

2.3 Bayesian Optimization

The general idea of Bayesian optimization is to construct a surrogate model that approximates a black box objective function, $f(x)$, and exploit this model to decide which points to evaluate next. The sampling strategy is determined by the choice of acquisition function, such as Expected Improvement (EI) and Lower Confidence Bound (LCB). Gaussian Process is commonly used as the surrogate model. For more detail about the Gaussian Process and a review of Bayesian optimization, see Rasmussen and Williams²⁷, Brochu *et al.*²⁸ and Shahriari *et al.*²⁹

$$\text{EI}(\theta) = \sigma(\theta)(z(\theta)\Phi(z(\theta)) + \phi(z(\theta))) \quad (3)$$

$$\text{LCB}(\theta) = \mu - \gamma\sigma(\theta) \quad (4)$$

Here, $z(\theta) = \frac{f(\theta_{\text{best}}) - \mu(\theta)}{\sigma(\theta)}$, where θ_{best} , $\mu(\theta)$, and $\sigma^2(\theta)$ are the best current value, predictive mean, and predictive variance respectively; while $\Phi(\cdot)$ and $\phi(\cdot)$ are the cumulative distribution function and probability density function, respectively; and γ is a parameter to balance exploration against exploitation. We should note that the acquisition functions (Eq. 3 and 4) take model uncertainty into account when selecting next query points, but it is still possible to select points in regions with steric clashes. In this work, we therefore define a new acquisition function that makes use of our domain knowledge, namely Knowledge-based Expected Improvement (KEI), to address this problem.

2.3.1 Knowledge-based Expected Improvement

Knowledge-based Expected Improvement (KEI) can be considered as a modified expected improvement (EI) acquisition function that offers improvement only when a set of torsion constraints are satisfied:

$$a_{\text{KEI}}(\theta) = \text{EI}(\theta) \prod_{m=1}^M P_m(\theta_{m,1}, \theta_{m,2}) \quad (5)$$

where M is the total number of correlated torsions found in the molecule, $P_m(\theta_{m,1}, \theta_{m,2})$ is the mixture model of the torsion angle pairs in pattern, m . We assume independence between each pair of correlated torsions. The idea of KEI is similar to the method of expected improvement with Boolean constraints suggested by Griffiths and Hernández-Lobato, and Gelbart *et al.*, with a user-specified minimum confidence of the constraints.^{30,31} Instead of Boolean constraints, we derived separate distributions of the correlated torsions from the lowest energy conformations found by MMFF94, and GFN2. These were encapsulated by bivariate von Mises mixture models, which are used to constrain the search.

2.3.2 Covariance Function

Since potential energy is known to be periodic with respect to dihedral angle, a locally periodic kernel, k_{LP} , which is a product of a periodic kernel and a squared exponential kernel, was used:

$$k_{LP}(\theta, \theta') = \sigma^2 \exp\left(-\frac{\|\theta - \theta'\|^2}{2l^2}\right) \exp\left(-\frac{2 \sin^2(\pi|\theta - \theta'|/p)}{l^2}\right) \quad (6)$$

where l , p , and σ^2 are the length-scale, periodicity, and variance, respectively. The periodicity is determined by torsional potentials corresponding to the rotatable bond SMARTS patterns. Note that for missing patterns that did not match a specific type of rotatable bond, *i.e.* did not match a SMARTS pattern, we assigned general values for the periodicity based on the atomic hybridization of the two atoms in the central rotatable bond, *i.e.* $sp^2 - sp^2$, $sp^2 - sp^3$, or $sp^3 - sp^3$. Boundary constraints were added to the length-scale in the kernel for numerical stability.

2.4 Data

We used two datasets, the Platinum dataset,³ and a dataset assembled by Ebejer *et al.*³², to benchmark the performance of the search algorithms. Duplicated molecules in the two datasets were removed based on their InChI Key. Molecules with 2 to 18 rotatable bonds, and containing two adjacent rotatable bonds matching the set of rotatable bond-SMARTS patterns, were selected for the study, giving a set of 533 unique molecules.

We extracted small molecules with matching rotatable bonds from the Crystallography Open Database (COD), and removed duplicate molecules from the COD set that were present in both the validation set and COD based on their InChI Key. We recorded the torsional preferences in these crystal structures. In addition, we calculated the lowest energy conformations of these molecules using MMFF94 and GFN2, and recorded the resultant calculated torsional preferences for each. We then derived bivariate von Mises mixture models from the torsional preferences found in X-

ray crystal structures, and calculated by the MMFF94 and GFN2 methods.

2.5 Evaluation

2.5.1 Energy function

Previously⁶, we computed a single-point MMFF94 force field energy while keeping the small molecule's bond lengths and bond angles fixed. Here, we relaxed the framework and evaluated the energy of the fully-optimized molecule, *i.e.* the energy value at a given set of dihedral angles was a result of a short (50 steps) MMFF94 energy minimization, with a concomitant change in bond lengths and bond angles, while the torsion angles remained fixed during geometry optimization. We used the MMFF94 implementation in Open Babel 2.4.1³³. The configurations in the benchmark datasets were used as the initial structures.

In addition, we performed single-point energy calculations with a more accurate semi-empirical method, namely GFN2^{21,22}. Similarly, the configurations in the benchmark datasets were used as initial structures. The bond length, bond angles and other parameters were inherited from the input structures.

2.5.2 Comparison

Three global optimization conformational search methods were compared using the same, fixed number of energy evaluations: (i) a Genetic Algorithm (GA), and our Bayesian Optimization Algorithm, BOA, with two different acquisition functions: (ii) our previous expected improvement (EI) method,⁶ and (iii) the new knowledge-based expected improvement (KEI) strategy. The implementations are described below.

(i) *Bayesian Optimization with EI (BOA-EI)*⁶. GPyOpt³⁴ was used for the Bayesian optimization and Pybel³⁵ was used to drive the torsion angles of the molecules and energy minimization. Note that torsion constraints were used in the geometry optimization step (*i.e.*, minimization of all other degrees of freedom, bonds, angles, etc. with fixed dihedral angles). Expected improvement was used as the acquisition function. Five initial random samples were generated to begin a Gaussian Process regression. We also added boundary constraints to the length-scale parameter for the sake of numerical stability. The lowest energy conformation calculated from all iterations returned as the final output structure.

(ii) *Bayesian Optimization with KEI (BOKEI)*. The implementation was the same as the standard Bayesian optimization in (i), except a knowledge-based acquisition function, KEI, was used.

(iii) *Genetic Algorithm (GA)*. The implementation in Open Babel³³ for GA was used. The GA search terminated when either the maximum number of energy evaluations was reached or three identical generations were observed; all other GA parameters were left as their default values. Note that no torsion constraints were added in the energy minimization step as the surrogate model was not required.

2.6 Search Space

The search space for each molecule is determined by its set of freely-rotatable bonds. The search space for the Bayesian optimization and its variant was defined by the hypercube $[-\pi, \pi)^d$, where d is the number of rotatable bonds. A discrete grid space was used for GA.

2.6.1 Search Budget

The number of energy evaluations was determined by the number of rotatable bonds in the molecule (see Table 1). Since five initial samples were used to fit a Gaussian process in Bayesian optimization, only $K - 5$ conformations were sampled after initial sampling. For accurate statistical comparisons of these stochastic methods, five runs were performed for each algorithm.

Table 1 Sample size versus number of rotatable bonds

Number of rotatable bonds	Number of conformers (K)
2-3	25
4-5	50
6-7	100
≥8	200

2.6.2 Analysis

Energy difference (ΔE) between the lowest energy conformation obtained by other methods and that from BOA-EI was calculated. The average energy difference was used to evaluate the performance of the search methods. The average energy difference is calculated as follows:

$$\overline{\Delta E^{KEI}} = \frac{1}{N} \sum_{i=1}^N (E_{KEI,i} - E_{EI,i}) \quad (7)$$

$$\overline{\Delta E^{GA}} = \frac{1}{N} \sum_{i=1}^N (E_{GA} - E_{EI,i}) \quad (8)$$

where N is the number of runs. $E_{EI,i}$ and $E_{KEI,i}$ are the lowest energy found by EI and KEI in i -th run respectively. E_{GA} is the lowest energy conformation found in all runs (do not depend on i -th run). The lowest energy conformation found by BOA-EI was used as reference in both cases. Since same initialization was used in both BOKEI and BOA-EI, *i.e.* five initial samples were the same, we could directly compare the performance between them in each run. In GA, We compared its best performance to each run in BOA-EI. Two different energy functions were used in the context and we denote $\overline{\Delta E_{MMFF94}}$ and $\overline{\Delta E_{GFN2}}$ to be the average energy difference in MMFF94 and GFN2 respectively.

Wilcoxon signed-rank test was used to test whether the proposed method, BOKEI, finds lower average energy conformations than BOA-EI and GA, *i.e.* one-sided test. We tested it across a varying number of rotatable bonds with both MMFF94 and GFN2 energy functions.

Furthermore, we calculated the frequency of BOKEI in finding lower energy conformations than BOA-EI and GA. We also computed the pattern frequency of our derived torsions pattern across three datasets, namely Platinum dataset³, COD, and ChEMBL 25³⁶, and compared to that of the correlated torsion patterns de-

finied in CSD Conformer Generator⁹.

Lastly, we performed run time analysis on BOA-EI and BOKEI, using a desktop running Fedora 30 with an Intel Core i7-6700 operating at 3.40 GHz, and 32 GB of RAM. Single core was used to read molecule, drive torsions and write conformers to disks. All cores were used in the GPyOpt operations. The time included reading input molecules and writing the conformers to disk. Fifteen molecules with two to six rotatable bonds, three for each, were sampled. We repeated the search with four times for each molecule.

3 Results and Discussion

3.1 Example

Two molecules were sampled to illustrate the strengths and the weaknesses of the BOKEI algorithm, using the geometry-optimized MMFF94 energy (see Appendix 3 for more examples with GFN2). Ten runs were performed for each molecule. From Fig.2, we can see BOKEI is able to find lower energy conformation consistently using same number of iterations. The energy gap between BOKEI and BOA-EI decreased as the number of iterations increased, since both methods should converge to the same global minimum. We should note that the performance of BOKEI was worse than BOA-EI in this example 2b, which was a result of under-estimation of the correlated torsion distribution. Insufficient sampling or biased selection of molecules gave rise to the incomplete prior information, and led to the inferior performance. Using additional data to improve the correlated distributions, even in this case, the performances became similar, as discussed in Section 3.7.

We revisited the example, 5-Phenylthioquinazoline-2,4-diamine, and studied the effect of the new acquisition function on the posterior. Fig.S5 in Appendix 2 shows that the posterior of BOA-EI and BOKEI after twenty iterations (25 observations in total, with five initial samples). GFN2 energy function was used in this example. The posterior mean showed a coarse boundary between high and low energy regions. The observations in BOKEI were more closely packed in the low energy region, compared to that in BOA-EI. Only a small number of observations were sampled in medium or high energy region, the posterior standard deviations thus remained high.

3.2 Dataset Summary

For a broader comparison, 533 molecules ranging from 2–18 rotatable bonds were used to validate the performance. In GFN2, we benchmarked the performance with molecules up to 13 rotatable bonds only. The number of matches for each pattern in the validation set is summarized in Appendix 3 Fig. S7. Five correlated SMARTS patterns are frequently found, with frequency greater than 100. Note that there were nine molecules (five in MMFF94 and four in GFN2) excluded from analysis due to early stopping in one of the five runs (see Appendix 4 Table S8 and S9). This was manifested by a non-positive definite kernel error.

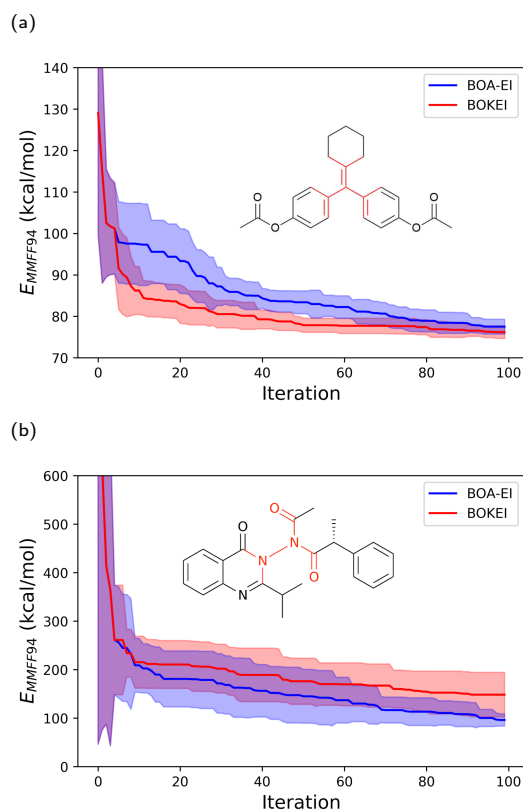


Fig. 2 The red line and the blue line in the convergence plots represents average rate of the BOKEI and BOA-EI in finding lower energy conformations respectively, with ± 1 sample standard deviation (shaded region). The corresponding molecule and the correlated torsion is highlighted in red. Geometry-optimized MMFF94 energy function was used in both cases. More examples with GFN2 energy function can be found in Appendix 3 Fig.S4. (a) BOKEI consistently finds lower energy conformations than BOA-EI in early stage and the energy gap reduces as the number of iterations increased. (b) Unusually, BOKEI performs worse than BOA-EI, which is a result of under-estimation of the correlated torsion.

3.3 MMFF94

Fig. 3a shows that BOKEI consistently finds lower energy conformation than BOA-EI and GA. A Wilcoxon signed rank test shows that energy difference between BOKEI and BOA-EI is statistically significant ($p < 0.01$, see Appendix 3 Table S4) across all rotatable bonds. On the other hand, we can see that the GA outperforms BOKEI and BOA-EI for molecules with more than twelve rotatable bonds. This is because the small number of samples (200 energy evaluations) may not be sufficient for the BOA-EI or BOKEI models to learn the most likely dihedral angles in high dimensional problems. Fig. S6a in Appendix 3 shows that BOKEI frequently ($> 63\%$ and $> 70\%$) finds lower energy conformations than BOA-EI and GA for molecules with fewer than eleven rotatable bonds respectively. Fig. S8a in Appendix 3 also shows that BOKEI gives a lower variation in energy than BOA of the output conformations in all five runs.

Furthermore, Fig. 2 highlights that BOKEI shows greater benefit in the early stage of the search. Comparing the mean energy difference between BOKEI and BOA-EI at different stages (40%,

60% and 100% of the maximum number of energy evaluations), the energy gap is indeed greater, and in favor of BOKEI, in the early stages (see Appendix 3 Table S6). The gap diminishes when more evaluations are used, since both methods converge to the same global optimum. These results suggest that the information about correlated torsions greatly helped the search in the early stage, pointing the search towards favorable regions of the potential energy landscape.

3.4 GFN2

In GFN2, we used a single-point energy calculation, and excluded GA in the analysis. Fig. 3b shows that BOKEI consistently finds lower energy conformations than BOA-EI. Similarly, Wilcoxon signed rank test shows the average energy difference between BOKEI and BOA-EI is statistically significant ($p \ll 0.01$, see Appendix 3 Table S5). The energy gap is greater in the early stage and the gap diminishes as more energy evaluations were used (see Appendix 3 Table S7). In addition, Fig. S6b in Appendix 3 shows that BOKEI frequently (> 60%) finds lower energy conformations than BOA-EI across all rotatable bonds. Fig. S8b in Appendix 3 shows that BOKEI gives a lower variation in energy than BOA of the output conformations in all five runs.

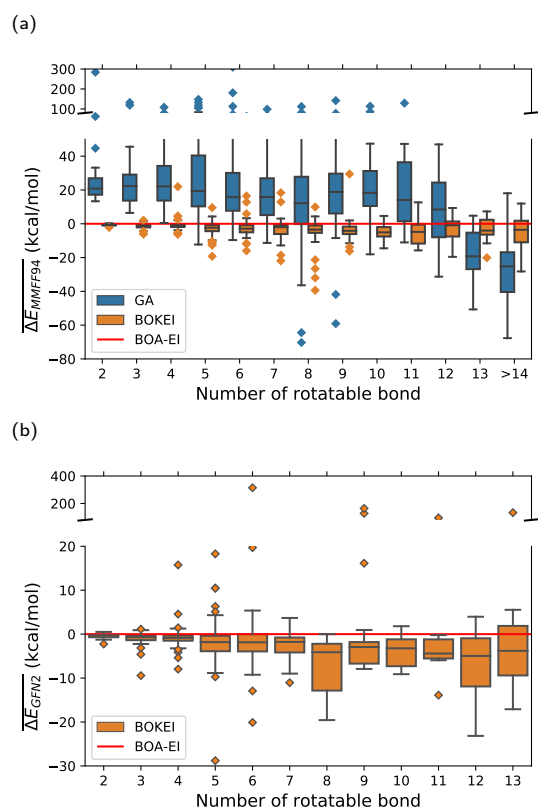


Fig. 3 (a): MMFF94 average energy difference from five runs. (b) GFN2 average energy difference from five runs. The average energy of the outputs from all runs found by BOA-EI is used as the reference point (red line) in (a) and (b). BOKEI often finds lower energy conformations than BOA-EI in both cases. The GA in MMFF94 outperforms BOKEI and BOA-EI for molecules with eleven or more rotatable bonds.

3.5 Correlated Torsion

When adjacent rotatable bonds have correlated dihedral angles, this is typically caused by unfavorable steric interactions — but not always. Four of the nineteen patterns in our library arise because of favorable intramolecular interactions, such as hydrogen bonds and π - π stacking. For example, in pattern 15, the lowest energy conformations found by GFN2 often form intramolecular hydrogen bonds between the N-H or O-H groups and the adjacent carbonyl oxygen atoms in the esters (see Fig. 4a).

The thioamide functional group is a key part of patterns 2 and 16 (see Fig. 4b). The delocalization of the nitrogen lone pairs in this group contributes to its overall planarity, but it could exist in either the *cis* or *trans* form. The orientation of the aromatic ring in pattern 2 is thus highly constrained. The *cis/trans* preference is easily revealed by examining higher-order correlated torsions, *i.e.* between three adjacent rotatable bonds. In particular, we considered a specific thiourea derivative that is bonded to a carbonyl group (see Appendix 1 Table S2). This is always observed to adopt the following conformation: (i) the C=S and C=O are oriented in 'opposite' directions, while (ii) the thiourea adopts the syn-anti³⁷ conformation. This results in the formation of a pseudo six-membered ring that is stabilized by a C=O \cdots H-N intramolecular hydrogen bond (see for example, Fig. 4b). Fig. S3 in Appendix 3 shows these three torsion angles are highly concentrated around 0° in COD.

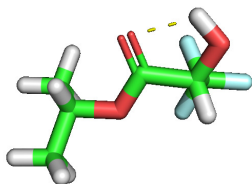
For pattern 17, π - π stacking is evident: when aromatic rings are attached to both ends of the pattern, both rings prefer to interact with one another (see Fig. 4c).

It should be noted that the CSD Conformer Generator⁹ also considers 11 correlated torsions, but a simple clash term is used for all other interactions. Here, we use a more flexible approach that employs bivariate von Mises mixture models to fully describe the correlated torsions. Both favorable intramolecular interactions and unfavorable steric clashes can be described. It would also be possible to expand this to a multivariate case³⁸, in order to capture higher-order correlations as mentioned earlier. Additionally, the framework is easy to integrate with other conformer sampling schemes, such as distance geometry^{17,26}. We intend to integrate with the ETKDG in RDKit in the future as the current implementation does not consider the correlated torsion.

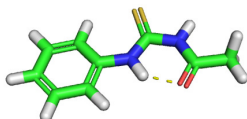
In addition, the torsional preference of MMFF94 differs from the one in GFN2 and crystal structures in pattern 1, 3 and 12. This suggests that some of the molecular interactions cannot be represented in classical force fields. In pattern 2, we notice a discrepancy between the crystal conformation and the lowest energy conformation in GFN2 – the second torsion angles (*i.e.* the torsion angles measured from the thioamide group) are highly concentrated around 180°, *i.e.* *trans*-form. This could be explained by the separate hydrogen bond interaction of the N-H group and the C=S in the crystal.

Furthermore, we compiled the number of the molecules with the presence of correlated torsions in three different datasets: (i) Platinum, (ii) COD and (iii) ChEMBL 25 (see Table 2). We found

(a)



(b)



(c)

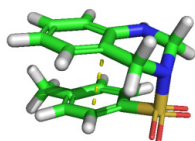


Fig. 4 Intramolecular H-bonds are observed in pattern 15 (a) and patterns 2 and 16 (b); while intramolecular π - π stacking is evident in pattern 17 (c).

that our SMARTS patterns library surprisingly matched 10 – 15% organic molecules, which was noticeably higher than the patterns defined in CSD Conformer Generator (1 – 4%). These results suggest that broader investigation of correlated torsions is warranted, despite the conventional assumption of each rotatable bond as an independent free rotor.

3.6 Computational Time

Fig. 5 shows the average run time of BOA-EI and BOKEI with GFN2 energy function, varying the number of iterations (50, 100) and number of rotatable bonds (two to six rotatable bonds). Both computational cost increases as the number of rotatable bonds increases. The computational time also increases when BOKEI is used, but is primarily dominated by the number of conformers generated. Note that the current implementation can be further optimized by providing the gradient information of the acquisition function.

In theory, extra multiplication in the BOKEI acquisition function increases the computational complexity of $O(mn)$, where m and n are the number of correlated torsion found in a molecule and the number of samples used to evaluate the acquisition function respectively. We should note that the relative contribution to the computational time of the new acquisition function will be small, when a more accurate and computational expensive method, such as density functional theory (DFT), is used for energy evaluation.

Our new algorithm will be more cost-effective than the old version in such settings.

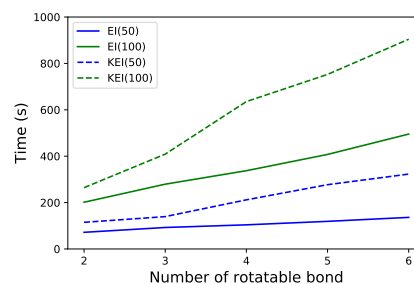


Fig. 5 Average computational time for BOA-EI and BOKEI with GFN2 energy function, using different number of energy evaluations (50, 100). The computational time increases as the number of rotatable bonds increase, but is dominated by the number of conformers generated.

3.7 Limitation and Future work

We only calculated the lowest energy conformation of the molecules with up to five rotatable bonds in the COD set, and the sampling of the low energy region of the correlated dihedral could be incomplete. This limited the performance of the algorithm. This issue can be easily solved by increase sampling of the corresponding substructures in a larger database, for instance ChEMBL³⁶ and PubChem³⁹, and re-estimating the distribution. Fig.6a showed the original prior used in Example 2b. We observed that the cluster centroids shifted when observations from ChEMBL were used (see Fig.6b), and Fig.6c showed a great improvement in convergence rate comparing to the original case.

In addition, hundreds of observations were typically required to fit the mixture models. Cole *et al.* derived a set of SMARTS patterns, and we did not use all of them due to insufficient observations. In order to overcome this obstacle, we could apply a meta-learning approach proposed by Ton *et al.*⁴⁰, which attempts to learn the conditional distribution of the correlated torsion. They showed that the approach could generalise the density of the correlated torsions with few observations. This meta-learning setting could greatly reduce the computational cost in learning torsion rules, and potentially help discover more unexpected torsion patterns for the sampling scheme.

4 Conclusions

By reformulating the search for the lowest energy conformation of a given molecule as a constrained Bayesian optimization problem, we have shown concrete improvements. Prior knowledge of correlated torsions was used to confine the exploration to regions of low energy. We compared the Bayesian optimization with two different acquisition functions: standard expected improvement (EI) and knowledge-based expected improvement (KEI), and genetic algorithm (GA), using two energy functions: MMFF94 and GFN2. We showed that with the same number of energy evaluations, the Bayesian optimization with KEI (BOKEI) frequently (> 60%) found lower energy conformations (median energy difference 1.95 kcal/mol in MMFF94 and 1.54 kcal/mol in GFN2) than the Bayesian optimization with EI (BOA-EI) in both cases,

Table 2 Frequency of molecules with the presence of correlated torsion patterns, comparing this work to previous steric constraints⁹ across various databases, including the Crystallographic Open Database (COD).

Dataset	Number of Molecules	% Matches (New)	% Matches (CSD)
Platinum	4,548	9.2	2.5
COD	110,623	13.5	1.6
ChEMBL 25	1,870,461	14.6	3.6

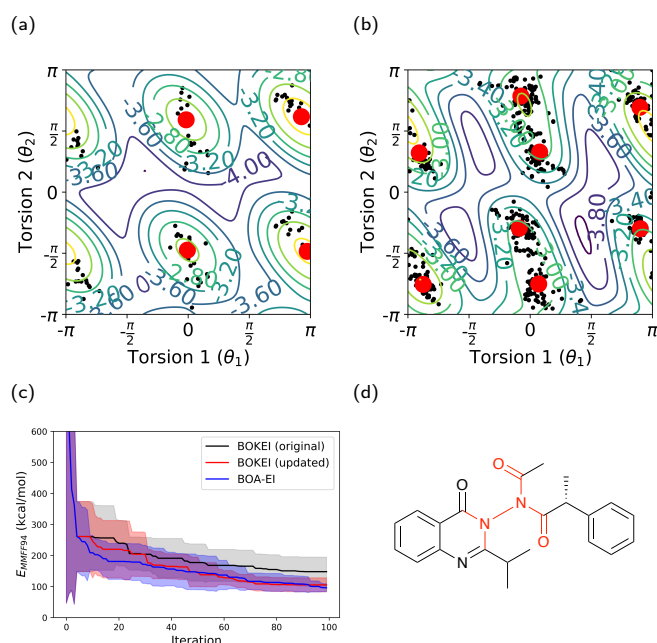


Fig. 6 (a) Mixture model derived from the COD dataset. (b) Mixture model derived from COD and ChEMBL database. The contour plot indicates the log density of a mixture model and the points (in red) mark the mean location for the components. (c) Convergence plot. (d) Molecule used to validate the performance of the updated prior.

across all rotatable bonds.

Importantly, using bivariate von Mises mixture models to describe the correlated dihedral allowed us to capture correlation that could not be explained by simple clash terms, and this approach could be integrated into other conformer sampling frameworks easily. Furthermore, we showed that the correlated torsions not only reflect steric clashes, but also favorable intramolecular interactions such as hydrogen bonds and π - π stacking.

Future work should focus on expanding data sources, to ensure sufficient sampling across a wide range of correlated dihedrals including other types of neighbors, non-nearest neighbors. Moreover, ring torsions were not investigated, which are well-known to involve correlations torsional motion (e.g. Cremer-Pople angles and ring pucker)^{41,42}. Such efforts will improve the efficiency in sampling low-energy conformers for applications in property-driven drug design, materials screening, and crystal structure prediction.

Conflicts of interest

There are no conflicts to declare.

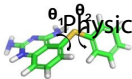
Acknowledgements

GRH thanks the National Science Foundation (CHE-1800435) for support. GMM thanks the EPSRC and MRC for financial support under grant number EP/L016044/1. The authors would like to acknowledge the use of the University of Oxford Advanced Research Computing (ARC) facility in carrying out this work, and supported in part by the University of Pittsburgh Center for Research Computing through the computational resources provided. We also thank Prof. Jotun Hein, Susan Leung and Carlos Outeiral for helpful discussion.

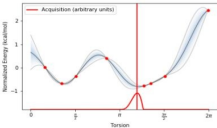
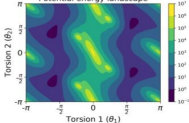
Notes and references

- 1 P. C. D. Hawkins, *Journal of Chemical Information and Modeling*, 2017, **57**, 1747–1756.
- 2 N.-O. Friedrich, C. de Bruyn Kops, F. Flachsenberg, K. Sommer, M. Rarey and J. Kirchmair, *Journal of Chemical Information and Modeling*, 2017, **57**, 2719–2728.
- 3 N.-O. Friedrich, A. Meyder, C. de Bruyn Kops, K. Sommer, F. Flachsenberg, M. Rarey and J. Kirchmair, *Journal of Chemical Information and Modeling*, 2017, **57**, 529–539.
- 4 S. Grimme, C. Bannwarth, S. Dohm, A. Hansen, J. Pisarek, P. Pracht, J. Seibert and F. Neese, *Angewandte Chemie International Edition*, 2017, **56**, 14763–14769.
- 5 S. Grimme, *Journal of Chemical Theory and Computation*, 2019, **15**, 2847–2862.
- 6 L. Chan, G. R. Hutchison and G. M. Morris, *Journal of Cheminformatics*, 2019, **11**, 32.
- 7 N. M. O'Boyle, T. Vandermeersch, C. J. Flynn, A. R. Maguire and G. R. Hutchison, *Journal of Cheminformatics*, 2011, **3**, 8.
- 8 J. R. Gardner, G. Pleiss, D. Bindel, K. Q. Weinberger and A. G. Wilson, *Advances in Neural Information Processing Systems*, 2018.
- 9 J. C. Cole, O. Korb, P. McCabe, M. G. Read and R. Taylor, *Journal of Chemical Information and Modeling*, 2018, **58**, 615–629.
- 10 N.-O. Friedrich, F. Flachsenberg, A. Meyder, K. Sommer, J. Kirchmair and M. Rarey, *Journal of Chemical Information and Modeling*, 2019, **59**, 731–742.
- 11 S. Kothiwale, J. L. Mendenhall and J. Meiler, *Journal of Cheminformatics*, 2015, **7**, 47.
- 12 P. C. Hawkins, A. G. Skillman, G. L. Warren, B. A. Ellingson and M. T. Stahl, *J Chem Inf Model*, 2010, **50**, 572–84.
- 13 H. M. Berman, J. Westbrook, Z. Feng, G. Gilliland, T. N. Bhat, H. Weissig, I. N. Shindyalov and P. E. Bourne, *Nucleic Acids Research*, 2000, **28**, 235–242.
- 14 C. R. Groom, I. J. Bruno, M. P. Lightfoot and S. C. Ward, *Acta*

- Crystallographica Section B*, 2016, **72**, 171–179.
- 15 W. Guba, A. Meyder, M. Rarey and J. Hert, *Journal of Chemical Information and Modeling*, 2016, **56**, 1–5.
 - 16 G. Landrum, *RDKit: Open-Source Cheminformatics*, 2018, <http://www.rdkit.org>.
 - 17 S. Riniker and G. A. Landrum, *Journal of Chemical Information and Modeling*, 2015, **55**, 2562–2574.
 - 18 S. Gražulis, D. Chateigner, R. T. Downs, A. F. T. Yokochi, M. Quirós, L. Lutterotti, E. Manakova, J. Butkus, P. Moeck and A. Le Bail, *Journal of Applied Crystallography*, 2009, **42**, 726–729.
 - 19 S. Gražulis, A. Daškevič, A. Merkys, D. Chateigner, L. Lutterotti, M. Quirós, N. R. Serebryanaya, P. Moeck, R. T. Downs and A. Le Bail, *Nucleic Acids Research*, 2012, **40**, D420–D427.
 - 20 T. A. Halgren, *Journal of Computational Chemistry*, 1996, **17**, 490–519.
 - 21 S. Grimme, C. Bannwarth and P. Shushkov, *Journal of Chemical Theory and Computation*, 2017, **13**, 1989–2009.
 - 22 C. Bannwarth, S. Ehlert and S. Grimme, *Journal of Chemical Theory and Computation*, 2019, **15**, 1652–1671.
 - 23 K. V. Mardia, C. C. Taylor and G. K. Subramaniam, *Biometrics*, 2007, **63**, 505–512.
 - 24 W. Boomsma, K. V. Mardia, C. C. Taylor, J. Ferkinghoff-Borg, A. Krogh and T. Hamelryck, *Proceedings of the National Academy of Sciences of the United States of America*, 2008, **105**, 8932–7.
 - 25 K. V. Mardia and J. Frellsen, in *Statistics of Bivariate von Mises Distributions*, ed. T. Hamelryck, K. Mardia and J. Ferkinghoff-Borg, Springer Berlin Heidelberg, Berlin, Heidelberg, 2012, pp. 159–178.
 - 26 D. C. Spellmeyer, A. K. Wong, M. J. Bower and J. M. Blaney, *Journal of Molecular Graphics and Modelling*, 1997, **15**, 18 – 36.
 - 27 C. E. Rasmussen and C. K. I. Williams, *Gaussian Processes for Machine Learning*, The MIT Press, Cambridge, Massachusetts, 2006.
 - 28 E. Brochu, V. M. Cora and N. de Freitas, *CoRR*, 2010, [abs/1012.2599](https://arxiv.org/abs/1012.2599), year.
 - 29 B. Shahriari, K. Swersky, Z. Wang, R. P. Adams and N. de Freitas, *Proceedings of the IEEE*, 2016, **104**, 148–175.
 - 30 R.-R. Griffiths and J. M. Hernández-Lobato, *arXiv e-prints*, 2017, arXiv:1709.05501.
 - 31 M. A. Gelbart, J. Snoek and R. P. Adams, *Proceedings of the 30th Conference on Uncertainty in Artificial Intelligence*, 2014, pp. 250–259.
 - 32 J.-P. Ebejer, G. M. Morris and C. M. Deane, *Journal of Chemical Information and Modeling*, 2012, **52**, 1146–1158.
 - 33 N. M. O’Boyle, M. Banck, C. A. James, C. Morley, T. Vandermeersch and G. R. Hutchison, *Journal of Cheminformatics*, 2011, **3**, 33.
 - 34 G. Authors, *GPyOpt: A Bayesian Optimization framework in Python*, <http://github.com/SheffieldML/GPyOpt>, 2016.
 - 35 N. M. O’Boyle, C. Morley and G. R. Hutchison, *Chemistry Central Journal*, 2008, **2**, 5.
 - 36 A. Gaulton, A. Hersey, M. Nowotka, A. P. Bento, J. Chambers, D. Mendez, P. Mutowo, F. Atkinson, L. J. Bellis, E. Cibrián-Uhalte, M. Davies, N. Dedman, A. Karlsson, M. P. Magariños, J. P. Overington, G. Papadatos, I. Smit and A. R. Leach, *Nucleic Acids Research*, 2016, **45**, D945–D954.
 - 37 S. Sahu, P. Rani Sahoo, S. Patel and B. Mishra, *Journal of Sulfur Chemistry*, 2011, **32**, 171–197.
 - 38 K. V. Mardia, G. Hughes, C. C. Taylor and H. Singh, *The Canadian Journal of Statistics / La Revue Canadienne de Statistique*, 2008, **36**, 99–109.
 - 39 S. Kim, J. Chen, T. Cheng, A. Gindulyte, J. He, S. He, Q. Li, B. A. Shoemaker, P. A. Thiessen, B. Yu, L. Zaslavsky, J. Zhang and E. E. Bolton, *Nucleic Acids Research*, 2018, **47**, D1102–D1109.
 - 40 J.-F. Ton, L. Chan, Y. W. Teh and D. Sejdinovic, *arXiv e-prints*, 2019, arXiv:1906.02236.
 - 41 D. Cremer and J. A. Pople, *Journal of the American Chemical Society*, 1975, **97**, 1354–1358.
 - 42 A. D. Hill and P. J. Reilly, *Journal of Chemical Information and Modeling*, 2007, **47**, 1031–1035.



Potential energy landscape



Global minimum